Ocean Sci. Discuss., 7, 1059–1102, 2010
www.ocean-sci-discuss.net/7/1059/2010/
doi:10.5194/osd-7-1059-2010

Ocean Science Discussions

Estimates of radiance reflected towards the zenith at the surface of the sea

E. Aas

Department of Geosciences, University of Oslo, Norway

Received: 6 April 2010 – Accepted: 28 May 2010 – Published: 14 June 2010

Correspondence to: E. Aas (eyvind.aas@geo.uio.no)

Published by Copernicus Publications on behalf of the European Geosciences Union.

Abstract

Remote sensing of water colour by ship-mounted sensors represents an important tool for the validation of satellite products and the monitoring of water quality. The recorded radiance from the sea has to be corrected for the surface-reflected radiance from sun and sky in order to obtain the water-leaving radiance. Here the simple case of radiance reflected towards the zenith is studied. A set of observed sky radiance and solar irradiance data from Oslo has been used together with a Gaussian slope distribution for the sea surface in order to estimate the reflected radiance. The spectral range studied is 405–650 nm, the solar zenith angles are in the range 37°–76°, and the wind speeds are up to 10 m s^{-1}. The analysis of the results show that the reflected radiance has to be separated into three contributions: sky radiance and sun rays reflected at the foam-free surface and irradiance reflected by whitecaps and foam. It is then demonstrated that by using four input values, namely the downward irradiance, the sky radiance from the zenith, the solar zenith angle and the wind speed, it is possible to obtain by simple expressions estimates of the reflected radiance that only differ from the former calculated values by relative errors of 4% or less. The analysis also indicates that for the spectral range studied neither the water-leaving radiance nor the surface-reflected radiance can be disregarded relative to the other one in the Case 2 waters of the Oslofjord-Skagerrak area. The results form a first step towards the study of reflected radiance in viewing angles differing from the nadir direction.

1 Introduction

Radiometric systems mounted on ships of opportunity have in recent years become an important tool for automatic monitoring of water quality. Real-time data are collected from several ferries in Norwegian coastal waters and adjacent areas (http://www.niva.no – Ferrybox monitoring). The analysis of these data would be improved if simple and accurate methods for the correction of reflected radiance existed.

OSD

7, 1059–1102, 2010

A ship-mounted radiance sensor looking down at the surface of the sea receives a radiance L_r consisting of light from the sky and sun reflected upwards at the surface, and a water-leaving radiance L_w consisting of light scattered upwards from different depths within the body of the water and transmitted through the water-air interface. Only the radiance L_w carries with it information about the optical properties of the water mass. If L_r can be estimated, then L_w can be found from the recorded total radiance L_r+L_w. One of the goals of remote sensing and marine optics is to develop methods by which it will be possible to determine the contents of optical components and the parameters of water quality from analysis of the water-leaving radiance.

The reflected radiance L_r is influenced by the wind speed, since the wind roughens the surface and eventually produces whitecaps and foam. The water-leaving radiance L_w, on the other hand, is practically independent of the wind, as will be demonstrated later in this paper. The relationship between wind speed and sea state was included in the Beaufort wind scale a century ago. The scale defines very characteristic features of the sea that are important for marine remote sensing. At Beaufort force 0 (calm, wind speed up to 0.3 m s^{-1}), the sea is flat. Ripples start to form at force 1 (light air, 0.3–1.5 m s^{-1}), and small wavelets are formed at force 2 (light breeze, 1.5–3.3 m s^{-1}). Wave crests start breaking at force 3 (gentle breeze, 3.3–5.5 m s^{-1}), producing scattered whitecaps, and the amount of whitecaps and foam increases at forces 4 and 5 (moderate and fresh breeze, 5.5–8 m s^{-1} and 8.0–11.0 m s^{-1}). In this paper the range of wind speed from 0 to 10 m s^{-1} is studied, since data from situations with stronger winds are not likely to be used.

The purpose of the present study is to see how L_r in the Skagerrak-Oslofjord area acts as a function of the solar zenith angle, the wind speed and the wavelength of light, and to determine if it is possible to estimate L_r with acceptable accuracy by indirect methods. Consequently the study is made as simple as possible, and the models for the statistical distribution of surface slope and for the influence of foam and whitecaps are chosen according to this principle. Because it simplifies the calculations only the radiance reflected towards zenith is studied. The reflected radiance L_r is decomposed

OSD
7, 1059–1102, 2010

into three parts: the reflected sky radiance $L_{r,sky}$, the reflected sun glints $L_{r,sun}$, and the light reflected from foam, $L_{r,foam}$.

Ship-mounted radiometers are usually given viewing directions that are optimal for avoiding the sun glitter. Mobley (1999) recommends a nadir angle of 40° and an azimuth angle of 135° away from the sun. In the present case with a viewing direction towards the nadir, more sun glints are received by the radiance meter, but the principles of the processes remain the same, and the much simpler and work-saving geometry justifies the chosen viewing direction. Our results are a first step toward methods of correction for other viewing angles.

Possible values of the ratio L_w/L_r are also investigated, because if $L_w/L_r \ll 1$, the accuracy of the estimated L_w will be too small to render L_w useful, and if $L_w/L_r \gg 1$, the influence of L_r on the recorded upward radiance can be neglected. However, while the magnitude of L_w is influenced by the optical properties of both the atmosphere and the sea, L_r is only influenced by the atmospheric properties. These two sets of optical properties are in no way correlated. Also the two data sets for L_r and L_w are independent and differ in time and space. Consequently, in order to make L_r and L_w comparable, they are normalized against the total downward irradiance E_{tot} from sun and sky in air and then L_w/L_r is estimated from the ratio of L_w/E_{tot} and L_r/E_{tot}.

2 Theoretical relationships and data material

2.1 The statistical distribution of slopes

The first comprehensive investigation of reflected light from a roughened sea surface was probably conducted by Cox and Munk (1954a, b). Recently Munk has pointed out several problems related to the roughness of the sea (Munk, 2009). A detailed discussion together with further references can be found in Walker (1994).

We will apply the notation of Cox and Munk (1954a, b) whenever practical. Let x designate the crosswind coordinate, y the upwind coordinate, and z the elevation of

OSD
7, 1059–1102, 2010

the surface, where z=0 describes the ocean at rest. Assume that a part of the surface is inclined relative to the horizontal surface, and let this part have an area vector of unit length at right angles to the area. This vector makes an angle β with the z-axis (Fig. 1), and β is also the angle between the surface and the horizontal plane z=0. The projection of the area vector into the x-y-plane has an azimuth angle α with the y-axis, where α is positive to the right of the upwind direction (Fig. 1). The direction of the projected area vector is then the direction where the slope is steepest. The slope of the inclined surface becomes m=tanβ. Let Δl be the projection of the area vector into the x-y-plane (Fig. 1) and Δz a height on the z-axis, related to m and Δl by

$$\frac{\Delta z}{\Delta l} = m = \tan\beta. \tag{1}$$

A line normal to Δl intersects the x- and y-axes at the two points

$$\Delta x = \Delta l / \sin\alpha, \qquad \Delta y = \Delta l / \cos\alpha. \tag{2}$$

The slopes of the surface in the x- and y-directions can be written by combining Eqs. (1) and (2)

$$z_x = \frac{\partial z}{\partial x} = \frac{\Delta z}{\Delta x} = \frac{\Delta z}{\Delta l}\sin\alpha = m\sin\alpha, \qquad z_y = \frac{\partial z}{\partial y} = \frac{\Delta z}{\Delta y} = \frac{\Delta z}{\Delta l}\cos\alpha = m\cos\alpha. \tag{3}$$

Evidently the sum of the two squared slopes z_x^2 and z_y^2 becomes

$$z_x^2 + z_y^2 = m^2\left(\sin^2\alpha + \cos^2\alpha\right) = m^2. \tag{4}$$

The mean values of the slopes in this equation can be written

$$\overline{z_x^2} + \overline{z_y^2} = \sigma_c^2 + \sigma_u^2 = \overline{m^2} = \sigma^2, \tag{5}$$

where σ_c^2 and σ_u^2 are the mean square slopes in the crosswind (x-) and upwind (y-) directions, and σ^2 the mean square slope.

OSD
7, 1059–1102, 2010

Cox and Munk found from observations of sun glitter that the statistical distribution of slopes in the x- and y-directions almost followed a two-dimensional Gaussian probability function. Their complete mathematical description can be simplified to a more approximate expression, and the distribution then becomes the Gaussian function

$$p(z_x, z_y) \approx \frac{1}{2\pi\sigma_c\sigma_u} \exp\left[-\frac{z_x^2}{2\sigma_c^2} - \frac{z_y^2}{2\sigma_u^2}\right]. \quad (6)$$

The slopes z_x and z_y have positive and negative values, and their mean values are zero. The double integral of $p dz_x dz_y$ between $-\infty$ and $+\infty$ along both horizontal axes is equal to 1.

In the data set obtained by Cox and Munk the ratio σ_c^2/σ_u^2 varied in the range 0.54–1.0 with a mean value of 0.75. The mean square slopes were linear functions of the wind speed W:

$$\sigma_c^2 = 0.003 + 0.00192\, W, \quad (7)$$

$$\sigma_u^2 = 0.000 + 0.00316\, W, \quad (8)$$

where W is the wind speed in $\mathrm{m\,s^{-1}}$. The mean square slope σ^2 was observed to be

$$\sigma^2 = \sigma_c^2 + \sigma_u^2 = 0.003 + 0.00512\, W. \quad (9)$$

The light reflected toward the zenith arrives from all azimuthal directions, and the measurements of radiance from the surface of the sea are taken for different azimuthal directions of the Sun. The probability distribution of the slopes has therefore been simplified to the one-dimensional case

$$p(m) = \frac{dN}{dm} \approx \frac{1}{(2\pi)^{0.5}\sigma} \exp\left[-\frac{m^2}{2\sigma^2}\right], \quad (10)$$

where dN is the fractional number of slopes of value m per slope unit dm. If we introduce the normalized slope

$$s = m/\sigma, \quad (11)$$

OSD
7, 1059–1102, 2010

the Gauss function obtains the form

$$p(s) = \frac{dN}{ds} \approx \frac{1}{(2\pi)^{0.5}} \exp\left[-\frac{s^2}{2}\right]. \quad (12)$$

The integral of $p\,ds = dN$ for s between $-\infty$ and $+\infty$ is equal to 1. The cumulated probability of the normalized slope being in the interval from $-\infty$ to s is expressed by

$$P(s) = \int_{-\infty}^{s} p(s')\,ds' = \int_{-\infty}^{s} \frac{1}{(2\pi)^{0.5}} \exp\left[-\frac{s'^2}{2}\right] ds', \quad (13)$$

and according to Abramowitz and Stegun (1970, Eq. 26.2.17) $P(s)$ can be approximated by

$$P(s) \approx 1 - p(s)\left[b_1 t + b_2 t^2 + b_3 t^3 + b_4 t^4 + b_5 t^5\right] \quad \text{where} \quad t = \frac{1}{1 + 0.2316419\,s} \quad (14)$$

b_1=0.319381530; b_2=−0.356563782; b_3=1.781477937; b_4=−1.821255978; b_5=1.330274429; with an error $<10^{-7}$.

A radiance from the zenith angle θ has an angle of incidence i at the surface and an angle of reflection r, where i=r. If the radiance is reflected towards zenith, then the sum i+r is equal to θ, or $\theta/2$=i=r. Moreover, the slope of the surface producing this reflection must have a slope angle β=i=r=$\theta/2$, as shown by Fig. 2. This means that slopes reflecting radiance towards zenith cannot be steeper than β=45°, and that s in our case is related to θ by

$$s = \frac{m}{\sigma} = \frac{\tan\beta}{\sigma} = \frac{\tan(\theta/2)}{\sigma} \quad . \quad (15)$$

The cumulative probability distribution for s being in the interval from $-s$ to s is expressed by $P(s)$−$P(-s)$. This distribution is presented in Fig. 3 for the wind speeds 0, 2, 5 and 10 m s^{-1}. Rather than using s as the variable along the horizontal axis, the related zenith angle θ of Eq. (15) has been applied. We see that 90% of the slopes

OSD
7, 1059–1102, 2010

reflecting radiance towards zenith corresponds approximately to directions of $\theta \leq 10^\circ$, 20°, 30° and 40° for the increasing wind speeds. That is, the higher the wind speed, the more parts of the sky contribute to the reflected radiance towards the zenith.

The upward radiance below the surface that is refracted and transmitted through the sloping surface towards zenith as the water-leaving radiance must have an angle j in water, relative to the normal to the surface, so that the corresponding refracted ray in air obtains the angle $\beta = r$ relative to the normal to the surface (Fig. 2). The relationship between j and β is expressed by Snell's Law:

$$\sin\beta = \sin r = n \sin j, \tag{16}$$

where n is the refractive index of sea water. Figure 2 shows that the zenith-directed radiance in air has a nadir angle in water, θ_w, related to β and j by

$$\theta_w = \beta - j = \beta - \arcsin\left(\frac{\sin\beta}{n}\right). \tag{17}$$

The corresponding cumulative distribution function $P(s) - P(-s)$ is shown in Fig. 4 for the wind speeds 0, 2, 5 and 10 m s^{-1}, as a function of the nadir angle in water, θ_w. This angle is related to the normalized slope s by Eqs. (15–17). The figure demonstrates that for wind speeds up to 10 m s^{-1}, 90% of the water-leaving radiance with a direction towards zenith is coming from nadir angles in water less than 6°.

2.2 Calculation of reflected sky radiance and sun glitter at the foam-free surface

For the present study it is useful to separate the reflected radiance L_r into the part consisting of reflected radiance from the sky, $L_{r,sky}$, the part consisting of reflected solar rays, termed the sun glitter, $L_{r,sun}$, and the part consisting of reflected radiance from both sky and sun, $L_{r,foam}$, reflected at the foam-covered parts of the surface. We will start by discussing the two first terms, since these are both functions of the slope distribution. Azimuthal mean values L of the sky radiance have been used since the slopes contributing to the reflected radiance are supposed to be oriented at random.

OSD
7, 1059–1102, 2010

The mean radiances were originally observed for the zenith angles 0°–15°–30°–45°–60°–75° by Høkedal and Aas (1998) and presented in tables.

From these tabulated values the mean radiances for each degree in the intervals have been interpolated, and in the range θ=75°–90° it has been assumed that the radiance is equal to L (75°). Then the mean values of L for the θ intervals 0°–1°, 1°–2°, 2°–3°, ..., 89°–90° have been calculated. A small increase of θ by $\Delta\theta$=1° corresponds to an increase of β by $\Delta\beta$=0.5°. Consequently the series θ=0°, 1°, 2°, ..., 90° has a series of reflecting surfaces with angles β=0°, 0.5°, 1°, 1.5°, ..., 45°. This produces a series of m by Eq. (1) and for a fixed wind speed a series of s by Eq. (11). The values of $P(s)$ have then been calculated for this series of s values. The probability ΔP that s should be in the interval from s_{n-1} to s_n is obtained by the subtraction

$$\Delta P = P(s_n) - P(s_{n-1}). \tag{18}$$

Thus for each interval $\theta \pm \Delta\theta/2$ there is a slope s that is able to reflect the radiance $L(\theta)$ towards the zenith, and ΔP is the weighting function for the radiance from θ. Instead of taking into account the negative values of s, only the positive values between 0 and ∞ have been used, and accordingly ΔP has been multiplied by 2. The sum of reflected sky radiances towards the zenith is therefore

$$L_{\mathrm{r,sky}} = \sum L(\theta)(2\Delta P)\rho_{\mathrm{a,w}}(\theta/2), \tag{19}$$

where the sum is for all the θ intervals 0°–1°, 1°–2°, 2°–3°, ... 89°–90°, and where $\rho_{\mathrm{a,w}}(\theta/2)$ is the Fresnel reflection at the air-water interface for an angle of incidence equal to $\theta/2$. The problem of polarization will be discussed in Sect. 3.1.

As a test it has been confirmed that

$$\sum (2\Delta P) = 1. \tag{20}$$

Since we are studying the radiance reflected towards the zenith, the azimuth angle between this direction and the position of the sun is undetermined. The tabulated values of the irradiance E_{sun0} of the direct solar rays on a plane normal to the rays

OSD
7, 1059–1102, 2010

(Høkedal and Aas, 1998) have accordingly been converted to equivalent azimuthal mean values of solar radiance. The angle of the solar diameter is approximately 0.5°, but since our calculations apply $\Delta\theta$=1°, it is practical to distribute the solar radiation within the solid angle $2\pi\sin(\theta_s)\,\Delta\theta$=0.10966$\sin(\theta_s)$, where θ_s is the solar zenith angle. The resulting equivalent solar radiance becomes

$$L_{sun}(\theta_s) = E_{sun0}/(0.1097\sin\theta_s). \quad (21)$$

The average contribution from the sun glitter can then be described by an expression similar to Eq. (19):

$$L_{r,sun} = L_{sun}(\theta_s)(2\Delta P)\rho_{a,w}(\theta_s/2). \quad (22)$$

2.3 Calculation of radiance reflected from the foam-covered part of the surface

It can easily be observed that the fraction F of the surface that is covered by foam and whitecaps from breaking waves increases with increasing wind speed W. The relationship between F and W has been discussed in several papers, e.g., Monahan (1971), Monahan and O'Muircheartaigh (1980, 1981, 1986), and Wu (1979). Monahan and O'Muircheartaigh (1980) obtained by the method of least squares the power-law

$$F = 2.95\cdot10^{-6}W^{3.52}, \quad (23)$$

where W is in units of m s^{-1}. The equation yields F=0.0098 for W=10 m s^{-1}. Thus less than 1% of the surface is covered by foam at wind speeds up to 10 m s^{-1}. In a later work Monaham and O'Muircheartaigh (1986) estimated F as a function of the temperature difference $\Delta T = T_{air} - T_{sea}$. Using monthly mean values of ΔT for the Færder Lighthouse at the northern border of the Skagerrak, the values of F become smaller than those obtained from Eq. (23). In the present study Eq. (23) is applied due to its simplicity.

Lauscher (1955) mentioned that foam of a sufficient thickness would reflect 50–80%. Whitlock et al. (1982) recorded the irradiance reflectance ρ_{f0} of foam in a laboratory tank and found that a reasonable constant value for the reflectance in the visible part

OSD
7, 1059–1102, 2010

of the spectrum at wavelengths of 440 nm and longer was ρ_{f0}=0.5±0.1. Also Frouin et al. (1996) obtained values of ρ_{f0} within the same range for breaking waves in the surf zone at La Jolla, California. In the open sea the foam reflectance seems to be smaller than in these investigations. Based on several series of photos from a research platform in the German Bight Koepke (1984) found that the time-averaged reflectance of the foam was $\rho_{f0}=0.22\pm0.11$ for wind speeds up to 10 m s^{-1}.

It is well established that the reflection from foam in the near infrared is smaller than in the visible part (Whitlock et al., 1982; Frouin et al., 1996; Moore et al., 1998, 2000; Nicolas et al., 2001; Kokhanovsky, 2004). The spectral variation in the visible part of the spectrum may depend on the thickness of the foam, according to Moore et al. (1998), who found that average reflectances at 410, 440, 510, 550, 670 and 860 nm were in the ranges 0.81–0.86, 1, 0.99–1.01, 0.98–0.99, 0.73–0.87, 0.38–0.59, respectively, when normalized at 440 nm. However, in a later work by the same authors (Moore et al., 2000) the reflectances seem to be constant from 410 to 670 nm, and then smaller at 860 nm. In this paper ρ_{f0} has been given the constant value 0.22 for the spectral range 405–650 nm. Visual observations of the foam in the Oslofjord-Skagerrak area, with its yellow substance-rich Case 2 waters, have indicated no spectral dependency.

Neglecting any bi-directional effects and assuming that the foam acts as a Lambertian emitter, ρ_{f0} can be related to the upward reflected radiance from the patch or streak of foam, $L_{r,foam,0}$, and the total downward irradiance in air, E_{tot}, by

$$\rho_{f0} = \pi L_{r,foam,0}/E_{tot}. \quad (24)$$

The foam-reflected radiance can then be written

$$L_{r,foam,0} = \frac{\rho_{f0}}{\pi} E_{tot}. \quad (25)$$

This radiance has to be weighted by the fractional area F of the foam in order to obtain the average contribution $L_{r,foam}$ to the total reflected radiance at the surface:

$$L_{r,foam} = F L_{r,foam,0} = F\frac{\rho_{f0}}{\pi} E_{tot}. \quad (26)$$

OSD
7, 1059–1102, 2010

If F can be expressed by Eq. (23) and ρ_{f0}=0.22, then Eq. (26) can be written

$$L_{r,foam} = F\frac{\rho_{f0}}{\pi}E_{tot} = (2.07\cdot 10^{-7}W^{3.52})E_{tot}. \quad (27)$$

Moore et al. (2000) used a radiometric system, deployed from a ship, in equatorial waters of the Pacific Ocean. Winds speeds were in the range from 9 to 12 m s^{-1}, and the data were collected during overcast conditions to avoid sun glints. Their augmented reflectance due to whitecaps and foam, $3.4\times10^{-6}W^{2.55}$, is close to the product $F\rho_{f0}$=$0.65\times10^{-6}W^{3.52}$ of Eq. (27) up to a wind speed of 7 m s^{-1}, but at stronger winds their reflectances are smaller.

2.4 Total reflected radiance at the surface

The total radiance reflected towards zenith at the surface of the sea can be written

$$L_r = (1-F)(L_{r,sky}+L_{r,sun})+FL_{r,foam,0}, \quad (28)$$

where the radiances have been weighted by their respective fractions of surface area. However, since $F\leq1\%$ according to Eq. (23) when $W\leq10$ m s^{-1}, Eq. (28) may without any significant loss of accuracy be simplified to

$$L_r = L_{r,sky}+L_{r,sun}+FL_{r,foam,0} = L_{r,sky}+L_{r,sun}+L_{r,foam}. \quad (29)$$

$L_{r,foam}$ is directly related to E_{tot} by Eq. (27), and $L_{r,sun}$ is related to E_{sun} by Eqs. (21–22). E_{tot} can be separated into the contributions from the diffuse sky irradiance E_{sky} and the direct solar irradiance E_{sun}

$$E_{tot} = E_{sky}+E_{sun}. \quad (30)$$

$L_{r,sky}$ and E_{sky} are both functions of the azimuthal mean values $L(\theta)$ of the sky radiance; $L_{r,sky}$ by Eq. (19), and E_{sky} by

$$E_{sky} = 2\pi\int_0^{\pi/2}L(\theta)\sin(\theta)\cos(\theta)d\theta = \pi\int_0^{\pi/2}L(\theta)\sin(2\theta)d\theta. \quad (31)$$

OSD
7, 1059–1102, 2010

All three terms of the reflected radiance L_r can then by calculated, provided $L(\theta)$, E_{sun0} or E_{sun}, and W have been recorded.

2.5 Calculation of water-leaving radiance

From the definition of radiance and Snell's Law it can readily be obtained that an upward radiance just beneath the surface, L_w^{0-}, produces a contribution ΔL_w to the water-leaving radiance by

$$\Delta L_w = L_w^{0-} \frac{\tau}{n^2}, \tag{32}$$

where τ is the transmittance of radiance through the water-air interface. The azimuthal mean value of L_w^{0-} from the nadir angle θ_w is denoted $L_w^{0-}(\theta_w)$. Assume that we know this mean value for all the θ_w intervals 0°–1°, 1°–2°, 2°–3°, ..., 89°–90°. This series of θ_w intervals corresponds to a series of β intervals determined by Eqs. (16)–(17). Note that although $\Delta\theta_w$ is constant, $\Delta\beta$ decreases with increasing θ_w due to Snell's Law. The new series of β intervals produces a series of m by Eq. (1) and for a fixed wind speed a series of s intervals by Eq. (11). For each s interval there is a probability ΔP for s being in this interval (Eq. 18).

The total water-leaving radiance is the sum of the contributions from all upward radiances in water, transmitted through the surface and refracted towards zenith:

$$L_w = \sum L_w^{0-}(\theta_w)(2\Delta P)\frac{\tau(j)}{n^2}. \tag{33}$$

The sum is for all the θ_w intervals 0–1°, 1–2°, 2–3°, ..., 89–90°, and $\tau(j)$ is the Fresnel transmittance at the water-air interface for an angle of incidence equal to j.

2.6 Observations of radiance and irradiance from sky and sun

A total of 52 data sets of angular distributions of sky radiance and direct solar irradiances, representing 9 different day with a clear sky, were collected in Oslo by Høkedal

OSD
7, 1059–1102, 2010

and Aas (1998) at the wavelengths 405, 450, 520, 550 and 650 nm, for solar zenith angles in the range 37–76°. The recordings were made manually by means of a tripod and a rotating Gershun tube provided with interference filters, often located on the roof of the high department building at the University of Oslo. The Gershun tube was of local construction (Aas, 1993), and its opening half-angle was 5.5° in order to ensure stable signals. Details of the calibration have been presented elsewhere (Aas, 1993). Measurements were taken over the upper hemisphere in steps of $\Delta\theta$=15° (range 0–75°) and $\Delta\alpha$=24–36° (range 0–180°). The time required for a complete recording with one filter was 15–20 min. During that time the solar zenith angle θ_s would have changed by 0° at noon, and 3° in the afternoon, implying that the atmospheric conditions could be regarded as practically constant for our purposes. A full spectral series took 80–90 min, corresponding to $\Delta\theta_s$=7–15°. The radiance $L(\theta,\alpha)$ and the solar irradiance E_{sun} were recorded directly by the Gershun tube, while E_{sky} was obtained by integration of $L(\theta,\alpha)$ (Eq. 31), and E_{tot} was then found by using Eq. (30). An earlier analysis of the results has been presented by Aas and Høkedal (1999).

2.7 Observations of sub-surface radiance and irradiance

During the Nordic Cruise to the Mediterranean in 1971 an extensive set of radiance and polarization data was collected onboard the R/V Helland-Hansen by Lundgren with an instrument constructed by the same person (Lundgren, 1971). The radiance sensor had an opening half-angle of 0.7°, and the wavelengths were in the range 405–502 nm. The sub-surface radiance field was recorded in steps of $\Delta\theta_w$=5–30°, while all azimuth angles were recorded in one continuous sweep of the instrument. The data were stored as graphs on paper rolls from printers. Through the years the recordings were read off and tabulated (Lundgren, 1971; Aas et al., 1997), and analyses were made (Højerslev and Aas, 1997; Aas and Højerslev, 1999; Adams et al., 2002).

Observations of radiance from nadir and upward and downward irradiance in the Oslofjord and Skagerrak, together with downward irradiance above the surface, have been collected by the Norwegian Institute for Water Research and the University of

OSD
7, 1059–1102, 2010

Oslo during several co-projects. The measurements have usually been taken onboard the R/V Trygve Braarud and G. M. Dannevig with the PRR-600 from Biospherical Instruments, San Diego, California, and the deck reference has been the PRR-601. The wavelengths are 412, 443, 490, 510, 555 and 665 nm, and the opening half-angle of the radiance sensor is 10° in water. The immersion coefficients provided by the manufacturer have been applied, and the self-shading effect (Gordon and Ding, 1992; Zibordi and Ferrari, 1995; Aas and Korsbø, 1997) has been accounted for. The upward radiance just beneath the surface, L_w^{0-}, was obtained by upward extrapolation from a depth of 0.5–1 m. This method requires that the vertical attenuation coefficient of the radiance is approximately constant within the upper meters of the surface layer. Factors like wave action, bubbles and accumulation of phytoplankton and detritus close to the surface may destroy the assumed constancy and thus influence the accuracy of the estimated L_w^{0-}, but as explained in another work (Aas et al., 2009), no clear signs of such influences have ever been found in the vertical profiles.

3 Results and discussion

3.1 $L_{r,sky}$, $L_{r,sun}$ and $L_{r,foam}$

The observations of sky radiance made by Hø kedal and Aas (1998) did not include the degree of polarization, except on two dates, and the reflectances were therefore calculated as if the radiance from the sky was unpolarized. This is certainly not correct. Their analyses showed that by neglecting the polarization the relative error of the reflected radiance for a flat sea might range from −39 to +14%. A negative error means that the calculated reflectance is less than the correct value. The reflected sky irradiance, based on radiances from the whole hemisphere, was underestimated by 2 to 5%. In the present analysis azimuthal mean values of the radiances are used, and a further analyses of the measurements show that the relative errors of the corresponding reflectances are in the range from −10 to +1% for radiances incident from zenith angles

OSD
7, 1059–1102, 2010

between 15 and 75°. If only zenith angles up to 45° are taken into account, then the range of the relative errors will be reduced, extending from −4 to +1% with a mean value of −2%. The slope distribution function ΔP (Eq. 18) gives more weight to the smaller values of θ than to the larger ones, as demonstrated by Fig. 5, and the polarization errors are smaller for the smaller values of θ. Figure 3, as already mentioned, shows that 90% of the contribution to the reflected radiance towards zenith comes from zenith angles less than 40° for wind speeds up to 10 m s^{-1}. Thus it seems reasonable to assume that on average our calculated reflectances may be underestimated by 2% due to the neglected polarization.

Kattawar and Adams (1990) used Monte Carlo simulations to study the effect of polarization on reflected and transmitted radiance at the surface of the sea. They found that errors up to 30% might occur in the radiances if the polarization was neglected. On the other hand, their results also showed that a positive error for one azimuth direction tended to be partly compensated for by a negative error for the opposite direction. The resulting errors of the azimuthal mean values of the radiances can be read off as ranging from 0 to 9%. Kattawar and Adams also found that the error of neglecting polarization effects in the calculation of irradiance reflected upwards at the surface was ≤2%. Consequently their model results support the field results of Høkedal and Aas.

Two factors influencing the amount of reflected light, especially for directions of incidence close to the horizon, are the processes of shadowing and multiple reflections. A facet of the surface may experience shadowing from other parts of the wave and from other waves, thus reducing the amount of reflected light. The process of multiple reflections, on the other hand, increases the reflectance for some directions. The influence of these effects on the upward-reflected light from the sea surface has been discussed by Preisendorfer and Mobley (1986) and Gordon and Wang (1992a,b). In the present paper the effects have not been taken into account, since more than 90% of the contributions to the zenith-reflected light comes from zenith angles less than 40° for wind speeds up to 10 m s^{-1}, that is from directions closer to the zenith than to the horizon.

OSD
7, 1059–1102, 2010

The 52 data sets described in Sect. 2.6 were used to calculate $L_{r,sky}$, $L_{r,sun}$ and $L_{r,foam}$, as expressed by Eqs. (19, 22 and 27), and L_r was then obtained by adding the three quantities (Eq. 29). The Fresnel reflectances were calculated for a refractive index of 1.340, corresponding to the average conditions of salinity, temperature and wavelength being approximately 30, 15 °C and 550 nm, respectively. The variation of the reflectances with regard to these three parameters is insignificant compared to the mentioned uncertainty introduced by the polarization.

3.2 The ratio L_r/L (0°)

In the NASA protocols it is suggested (Mueller et al., 2003) that L_r for a certain direction of observation 180°-θ can be estimated by recording the sky radiance in the same plane of incidence but from the opposite azimuth direction and the zenith angle θ, and multiplying the radiance by the corresponding Fresnel reflectance. In our case, the radiance reflected at the surface towards the zenith should be

$$L_r = L(0°)\rho_{a,w}(0°), \tag{34}$$

and the ratio L_r/L (0°) should become

$$L_r/L(0°) = \rho_{a,w}(0°) = 0.0211, \tag{35}$$

where $\rho_{a,w}(0°)$=0.0211 is the value of the Fresnel reflectance used in our calculations for a ray of normal incidence.

The results for the ratio $L_r/L(0°)$, calculated by Eqs. (19), (22), (27) and (29), and presented in Table 1, show that the estimate of $L_r/L(0°)$ found by Eq. (35) works well for a zero wind speed, since the ratio is within the range 0.0201–0.0220, with a mean value of 0.0215. The small deviations from a constant value are due to the mean square slope which is not zero even in the absence of wind, but 0.003 according to Eq. (9). When the wind speed W increases up to 10 m s^{-1}, the mean value of the ratio increases from 0.0215 to 0.0784, which is a factor 3.7 greater than the value 0.0211

OSD
7, 1059–1102, 2010

suggested by Eq. (35). In one case the ratio becomes 0.388, which is greater than 0.0211 by a factor of 18.

If we separate $L_r/L(0^\circ)$ into the components $L_{r,sky}/L(0^\circ)$, $L_{r,sun}/L(0^\circ)$ and $L_{r,foam}/L(0^\circ)$, we find that $L_{r,sky}/L(0^\circ)$ only ranges from 0.020 to 0.029 (Table 1). It also becomes clear that $L_{r,sun}/L(0^\circ)$ represents the smallest and greatest normalized reflectances toward the zenith (Table 1), ranging from 0 to 0.31. An interesting result is that the ratio $L_{r,sun}/L(0^\circ)$ is much smaller than $L_{r,sky}/L(0^\circ)$ for certain values of θ_s, as listed by Table 2. In these cases the contribution from sun glitter to the radiance directed towards the zenith can be neglected. Table 1 shows that the radiance reflected from foam can be neglected at a wind speed of $W=5\,m\,s^{-1}$, but contributes significantly to L_r (24% on an average) when $W=10\,m\,s^{-1}$. A closer examination of the data reveals that $L_{r,foam}/L(0^\circ)$ reaches the value of 0.001 at wind speeds between 5 and $7\,m\,s^{-1}$, implying that $L_{r,foam}$ should be taken into account whenever the wind speed is greater than $5\,m\,s^{-1}$. This is consistent with the sea state described by the Beaufort wind scale (Sect. 1). The ratio $L_{r,foam}/L_{r,sky}$ tends to decrease with increasing θ_s.

The results of Table 2 indicate that in the Northern Skagerrak, where the solar zenith angles $\theta_s \geq 37^\circ$, the method suggested by the NASA protocols is only valid when the wind speed is low ($W<2\,m\,s^{-1}$). At higher wind speeds ($W>2\,m\,s^{-1}$), Eq. (35) is only valid for a restricted range of θ_s, where the lower limit of the range increases with increasing wind speed. When the wind speed is $10\,m\,s^{-1}$, θ_s should be approximately 80° or greater in order to avoid sun glitter in the zenith direction. Table 2 also implies that in the Polar regions, where the sun is low, solar glitter is probably not a problem at moderate wind speeds when the direction of observation is close to the nadir.

Rather than using the constant reflectance 0.0211 to represent the ratio $L_r/L(0^\circ)$ in Eq. (35), we could approximate the ratios $L_{r,sky}/L(0^\circ)$, $L_{r,sun}/L(0^\circ)$ and $L_{r,foam}/L(0^\circ)$ by their respective bulk mean values for all solar zenith angles and wavelengths in the present data set, and test if that improved the results. Table 3 shows that the standard deviation from the mean value of $L_{r,sky}/L(0^\circ)$ is now less than 0.002 at wavelengths

OSD
7, 1059–1102, 2010

405, 450, 520, 550 and 650 nm, and for wind speeds up to 10 m s^{-1}. The maximum deviation of $L_{r,sky}/L(0^\circ)$ from the mean value in the obtained data set is less than 0.005. Data for $L_{r,sun}/L(0^\circ)$ where the values were much smaller than $L_{r,sky}/L(0^\circ)$, were not used in the statistical calculations of this ratio. Unfortunately the standard and maximum deviations for $L_{r,sun}/L(0^\circ)$ are still too great to be acceptable, amounting to 0.24 in the red part of the spectrum for W=10 m s^{-1}. The deviations of $L_{r,foam}/L(0^\circ)$ from the mean values at the different wavelengths are of the same order of magnitude as $L_{r,sky}/L(0^\circ)$ when W=10 m s^{-1}. Accordingly the use of the bulk mean value to estimate the ratios $L_{r,sun}/L(0^\circ)$ and $L_{r,foam}/L(0^\circ)$ is not a satisfactory method.

An additional experiment has been conducted by approximating the three ratios $L_{r,sky}/L(0^\circ)$, $L_{r,sun}/L(0^\circ)$ and $L_{r,foam}/L(0^\circ)$ by best-fit second order polynomials on the form $A+B_1\theta_s+B_2\theta_s^2$, where A, B_1 and B_2 are constants, for the different wavelengths and wind speeds. The errors are then reduced, but they are still too large for $L_{r,sun}/L(0^\circ)$ and $L_{r,foam}/L(0^\circ)$. At winds of 5 and 10 m s^{-1} the errors of $L_{r,sun}/L(0^\circ)$ amounted to 0.025 and 0.047, respectively, and at 10 m s^{-1} the errors of $L_{r,foam}/L(0^\circ)$ could reach 0.013. These errors are of the same order of magnitude as the mean values of $L_{r,sky}/L(0^\circ)$, 0.022–0.026, as shown by Table 1.

The ratio $L_{r,sky}/L(0^\circ)$ can be described with satisfactory accuracy by the mean values of Table 3, and by second order polynomials of θ_s. An additional useful property of the ratio is that if the value of $L_{r,sky}/L(0^\circ)$ is known at one wavelength, then this value can be applied to the other wavelengths as well. For instance, if the ratio is known at 405 nm, then the assumption that the ratio is the same at the other wavelengths, leads to relative RMS errors of 1–4–7% for the wind speeds 0–5–10 m s^{-1}, respectively. These errors are rather small compared to other errors connected with field measurements.

The different tests discussed here demonstrate that while the reflected sky radiance $L_{r,sky}$ is normalized in a useful way by the sky radiance $L(0^\circ)$, this normalization does not work for the sun glitter $L_{r,sun}$ and the foam-reflected $L_{r,foam}$. Consequently better

OSD
7, 1059–1102, 2010

normalizing quantities or reference inputs should be found for these two radiances. It was pointed out in Sect. 2.4 how $L_{r,foam}$ is related to E_{tot}, and $L_{r,sun}$ to E_{sun}. It was also mentioned that $L_{r,sky}$ is indirectly related to E_{sky}, since both quantities are functions of the sky radiance $L(\theta)$. A common normalizing quantity is unrealistic because there is no constant ratio between E_{sky} and E_{sun} at a given wavelength, wind speed or solar zenith angle. The ratio varies in an unpredictable way due to different optical conditions of the atmosphere, as displayed by Fig. 6. Here E_{sun}/E_{sky} varies by an order of magnitude, both in the violet (405 nm) and red (650 nm) parts of the spectrum. During the measurements of the two irradiances the solar zenith angle only varied by 0–3°, and the varying values of E_{sun}/E_{sky} shown by Fig. 6 must accordingly be due to variation of the atmospheric conditions from one day to another.

3.3 The ratios $L_{r,foam}/E_{tot}$, $L_{r,sun}/E_{sun}$ and $L_{r,sky}/E_{sky}$

At a given wind speed $L_{r,foam}$ is a linear function of E_{tot}, as shown by Eq. (27). The constant of proportionality is independent of the wavelength and solar angle, and depends only on the wind speed by a power-law.

The sun glitter $L_{r,sun}$ is related to E_{sun} by Eqs. (21–22), and both the wind speed and the solar angle influence its magnitude by means of the slope distribution function. The wavelength, however, has no practical influence, since the Fresnel reflectance of the surface is almost independent of wavelength. Accordingly $L_{r,sun}$ has been normalized by E_{sun}, and the ratio $L_{r,sun}/E_{sun}$ has been approximated by best-fit polynomials on the form $A+B_1\theta_s+B_2\theta_s^2$. We now find that the results are much more coherent than when the normalization was made by $L(0°)$, as can clearly be seen by comparing the results in Table 4. The striking fit between the polynomials and $L_{r,sun}/E_{sun}$ is shown by Fig. 7. The polynomials for sun glitter reflected in the zenith direction at the wind speeds 3, 5 and 10 m s^{-1} are presented in Table 5. An interesting and useful property of $L_{r,sun}/E_{sun}$ is that its value is independent of wavelength, so that if its value is known at one wavelength, then the value is also known at all other wavelengths. This could of course have been stated a priori.

OSD
7, 1059–1102, 2010

Similarly $L_{r,sky}$ has been normalized by E_{sky} in order to see whether the earlier results for $L_{r,sky}/L(0^\circ)$ can be improved. However, when $L_{r,sky}/E_{sky}$ is approximated by best-fit polynomials of θ_s, the overall errors of the resulting $L_{r,sky}$ are slightly greater than when $L_{r,sky}/L(0^\circ)$ was estimated in the same way. This is not surprising, since the sky radiances contributing to $L_{r,sky}$ have directions and values closer to $L(0^\circ)$ than the radiances from the whole hemisphere contributing to E_{sky}. Consequently, if $L(0^\circ)$ has been observed, the overall best estimates of $L_{r,sky}$ will be obtained by using the polynomials for $L_{r,sky}/L(0^\circ)$ (Table 5).

3.4 The ratio L_r/E_{tot}

If the downward irradiance E_{sun} and the downward radiance $L(0^\circ)$ have been observed, and the wind speed W and solar zenith angle θ_s are known, then it is possible to obtain estimates of $L_{r,sky}$ and $L_{r,sun}$ by the polynomials in Table 5. If, in addition, E_{tot} has been observed, $L_{r,foam}$ can be estimated by Eq. (27). The total reflectance L_r as well as the normalized total reflectance L_r/E_{tot} are then determined.

There is one objection that can be raised if one intends to apply this procedure to automatic recordings at sea, namely the problem of observing E_{sun}. While E_{tot} and $L(0^\circ)$ are easily measured by continuously recording sensors, the determination of E_{sun} is not a routine operation. It can be recorded manually by simple devices or automatically by high technology instruments, but such instruments are not suitable for mounting on a ship where they are exposed to varying weather conditions. The movements of the ship represent an additional problem. Fortunately, since E_{sky} is related to $L(0^\circ)$ by a hemispherical integral including $L(0^\circ)$, it is possible to estimate E_{sky} from the observed $L(0^\circ)$ with satisfactory accuracy. The use of second order polynomials of θ_s to approximate the ratio $E_{sky}/L(0^\circ)$ at the different wavelengths results in a relative RMS error of 6% for the estimated E_{sky}. The polynomials for $E_{sky}/L(0^\circ)$ are presented in Table 5. When E_{sky} has been estimated from $L(0^\circ)$ and θ_s, E_{sun} can be found by subtracting E_{sky} from the observed E_{tot}.

OSD
7, 1059–1102, 2010

The polynomials of Table 5 and Eq. (27) can now be applied to estimate the normalized reflectance towards zenith, L_r/E_{tot}. The complete procedure has been tested and compared to the directly calculated values of L_r/E_{tot} (Fig. 8). The RMS value of the errors by using the polynomials is ≤0.0001 at all wind speeds ≤10 m s^{-1}, while the relative errors are ≤4%.

It should be remembered that these errors represent the deviations between two methods based on the same input. Also, since the applied data set only represents 9 days with clear sky conditions, there may be situations that are not covered by the observations, and which could result in greater errors.

In the present study the applied wavelengths have been 405, 450, 520, 550 and 650 nm. These wavelengths are different from the channels of the satellite sensors MERIS, MODIS and SeaWiFS. However, based on the spectral distributions of L_r/E_{tot} found here, it seems that linear spectral interpolation of L_r/E_{tot} is a satisfactory method for obtaining values at other wavelengths.

The results at different wind speeds have mostly been presented for 0, 5 and 10 m s^{-1}. Comparison with results at other wind speeds indicates that L_r/E_{tot} may be interpolated as a linear function of W.

3.5 The ratio L_w/L_r

The azimuthal mean values $L_w^{0-}(\theta_w)$ of the sub-surface radiance can be converted to the water-leaving radiance L_w by Eq. (32). It was observed in Sect. 2.1 that for wind speeds up to 10 m s^{-1}, 90% of the directions contributing to L_w had nadir angles θ_w in water less than 6°. Within this small angular interval $L_w^{0-}(\theta_w)$ is practically constant. Tyler's (1960) observations of blue radiance in Lake Pend Oreille result in the value 1.03 for the ratio $L_w^{0-}(10°)/L_w^{0-}(0°)$ close to the surface. Based on linear interpolation the ratio $L_w^{0-}(5°)/L_w^{0-}(0°)$ should then have the value 1.015. Similar observations by Lundgren in the Mediterranean at a depth of 0.5–1 m (Aas et al., 1997) indicate values in a range from 1.00 to 1.01 for $L_w^{0-}(10°)/L_w^{0-}(0°)$, and even closer to 1.00 for

OSD
7, 1059–1102, 2010

$L_w^{0-}(5°)/L_w^{0-}(0°)$.

The data set of radiances and irradiances from the Oslofjord-Skagerrak area, described in Sect. 2.7, has been restricted to those 12 stations where 50% of the sky or more was free of clouds, and where θ_s was smaller than 76°. Because the instrument only records radiance from nadir, the radiance at other angles has to be estimated by other methods, like for instance the α model (Aas and Højerslev, 1999). This model approximates the azimuthal average $L_u(\theta_w)$ of upward radiance by the function

$$L_u(\theta_w) = L_u(0°)\frac{1+\alpha}{1+\alpha\cos\theta_w}, \quad (36)$$

where θ_w is the nadir angle in water, and α is defined by

$$\alpha = \frac{L_u(90°)}{L_u(0°)} - 1. \quad (37)$$

The Q factor is defined as the ratio between upward irradiance and nadir radiance, and by integrating Eq. (36) over the lower hemisphere it is readily found that

$$Q = 2\pi\frac{1+\alpha}{\alpha^2}[\alpha - \ln(1+\alpha)]. \quad (38)$$

Just beneath the surface Q exhibited values from 3.16 to 5.80, and by combining Eqs. (36–38), the estimates of $L_w^{0-}(10°)/L_w^{0-}(0°)$ become 1.01 ± 0.01, and for $L_w^{0-}(5°)/L_w^{0-}(0°)$ the deviations from 1.00 are less than 0.01. Thus the Case 2 waters of the Lake Pend Oreille and the Oslofjord-Skagerrak area, as well as the Case 1 waters of the Mediterranean, show that L_w^{0-} is practically constant for all nadir angles equal to or less than 10°.

It is therefore a reasonable approximation to make the substitution $L_w^{0-}(\theta_w) \approx L_w^{0-}(0°)$ in Eq. (33). The radiance transmittance $\tau(j)$ is 0.979 when θ_w is in the small range from 0 to 10°. By using n=1.340, Eq. (33) can then be approximated by

$$L_w \approx L_w^{0-}(0°)\frac{0.979}{1.340^2}\sum 2\Delta P = 0.545 L_w^{0-}(0°), \quad (39)$$

OSD
7, 1059–1102, 2010

since the sum of all probabilities is 1 (Eq. 20). It should be noted that the ratio $L_w/L_w^{0-}(0^\circ)$ is a constant value, independent of the wavelength and the wind speed. Aas et al. (2009) obtained the value 0.546 for this ratio by a different procedure, as an approximation for a flat sea.

The normalized water-leaving radiances L_w/E_{tot} have been calculated, and the results have been extrapolated and interpolated to the wavelengths used in this paper. The wind speed at the stations ranged from 1.5 to 7.5 m s^{-1}, with an average value and standard deviation equal to 4 and 2 m s^{-1}, respectively. For each station with a value of L_w/E_{tot} the atmospheric data that were closest with regard to θ_s were chosen, and the corresponding value of L_r/E_{tot} was then calculated for the same wind speed. The ratio between L_w/E_{tot} and L_r/E_{tot} may then provide a tentative estimate of L_w/L_r.

The results are presented in Table 6, which shows that L_w/L_r at the chosen stations on an average varies spectrally from 0.5 to in the UV to 0.7 in the red, with a maximum of 2 in the blue-green part. This means that the reflected radiance cannot be disregarded at any wavelength within the spectral range 405–650 nm, and that the contribution from the water-leaving radiance to the total upward radiance should not be disregarded either. That is, neither of the contributions from the surface of the sea to the radiance directed towards the zenith can be disregarded within this spectral range in the Oslofjord-Skagerrak area.

4 Summary and conclusions

The relationship between wind speed and mean square slope found by Cox and Munk (1954a, b) has been used with a one-dimensional Gaussian probability function for the surface slope in order to calculate the radiance from sky and sun reflected towards the zenith. The contribution $L_{r,sky}$ from the reflected sky radiance was expressed by Eq. (19), and the contribution $L_{r,sun}$ from the reflected sun glints by Eq. (22). The special contribution of reflected radiance from whitecaps and foam, $L_{r,foam}$, was calculated by Eq. (27), where the foam is assumed to act as a Lambertian emitter (constant

OSD
7, 1059–1102, 2010

radiance) with a spectrally constant reflectance. The input data have been the tabulated values of sky radiance, solar irradiance and total irradiance presented by Hø kedal and Aas (1998). The applied data set consisted of 52 sub-sets of angular distributions of sky radiance and direct solar irradiance in the Oslo region, at the wavelengths 405, 450, 520, 550 and 650 nm, and with solar zenith angles in the range 37–76°. From the calculated values of $L_{r,sky}$, $L_{r,sun}$ and $L_{r,foam}$ the total reflected radiance L_r could then be obtained.

Table 1 shows that the ratio $L_r/L(0^\circ)$ between the radiance reflected towards the zenith and the diffuse sky radiance incident from the zenith has no constant value for wind speeds in the range W=0–10 m s^{-1}. When W=0 m s^{-1}, the mean value of the ratio plus/minus the standard deviation is 0.0215 ± 0.0003, while the corresponding numbers for W=10 m s^{-1} are 0.0784 ± 0.0575. The mean value of the ratio has then increased by a factor of 3.7. This is due to the sun glitter that for certain solar zenith angles and wind speeds has a significant impact on the radiance reflected towards the zenith.

The results of Table 2 imply that the method of specular flat-ocean reflection expressed by Eq. (35) is only valid in our case with a zenith-directed reflectance and solar zenith angles in the range $\theta_s \geq 37^\circ$ when there is practically no wind, that is W<2 m s^{-1}. At wind speeds up to 5 m s^{-1} Eq. (35) can only be applied to a restricted range of θ_s where the lower limit of the range increases with increasing wind speed. When W=5 m s^{-1}, θ_s has to be 65° or greater in order to avoid significant effects of sun glitter in the zenith direction. The results of Table 1 show that the contribution of foam-reflected radiance should preferably be taken into account whenever $W \geq 5$ m s^{-1}, since it may then be in the range of 1–100% of $L_{r,sky}$.

In order to obtain simple but accurate methods for the estimation of the reflected radiance L_r, the radiance had to be separated into the three contributions $L_{r,sky}$, $L_{r,sun}$, and $L_{r,foam}$, with inputs from $L(0^\circ)$, E_{sun} and E_{tot}, respectively. Equation (27) provides a very simple relationship between $L_{r,foam}$, E_{tot} and W. The ratio $L_{r,sun}/E_{sun}$ can be approximated by best-fit polynomials on the form $A+B_1\theta_s+B_2\theta_s^2$, where A, B_1 and B_2

OSD
7, 1059–1102, 2010

are constants, and the results for the wind speeds 3, 5 and 10 m s^{-1} are presented in Table 5 and Fig. 7. These relationships are independent of wavelength. The ratio $L_{r,sky}/L(0^{\circ})$ has been described by similar polynomials for the different wavelengths and wind speeds, as shown by Table 5. Because there is no constant ratio between the different inputs at a given wavelength, wind speed and solar zenith angle, a common normalizing quantity for the three contributions to L_r is not possible. It has for instance been shown by Fig. 6 that the ratio E_{sun}/E_{sky} varies in an unpredictable way due to different optical conditions of the atmosphere.

While the measurements of $L(0^{\circ})$ and E_{tot} are standard operations, the separation of E_{tot} into E_{sky} and E_{sun} is not. It has been demonstrated, however, that it is possible to estimate E_{sky} from the observed $L(0^{\circ})$ with a relative RMS error of 6%, by using second order polynomials of θ_s. The polynomials for $E_{sky}/L(0^{\circ})$ are presented in Table 5. When E_{sky} has been estimated from $L(0^{\circ})$ and θ_s, E_{sun} can be found by subtracting E_{sky} from the observed E_{tot}.

Thus from known values of $L(0^{\circ})$, E_{tot}, W and θ_s, the reflected radiance L_r can be determined as described above. The results of this procedure have been presented in Fig. 8. The RMS value of the errors is $\leq$0.0001 at all wind speeds $\leq$10 m s^{-1}, while the relative errors are $\leq$4%, which should be an acceptable error.

Values of the ratio between the water-leaving radiance and the reflected radiance, L_w/L_r, have been tentatively estimated from field observations of L_w/E_{tot} and calculated values of L_r/E_{tot}. For the calculation of L_r/E_{tot} an atmospheric data set was chosen where θ_s was as close to the corresponding angle for L_w/E_{tot} as possible, and the calculation was made with the same wind speed as for L_w/E_{tot}. The wind speed at the selected stations varied from 1.5 to 7.5 m s^{-1} and the solar zenith angle from 37 to 52°. The results, presented in Table 6, show that within the spectral range 405–650 nm neither of the contributions L_w or L_r to the zenith-directed radiance can be disregarded relative to the other one in the Oslofjord-Skagerrak area.

This paper has discussed the case where the viewing direction has been directed towards the nadir. Ship-mounted sensors onboard a ship usually have non-nadir viewing

OSD
7, 1059–1102, 2010

angles in order to avoid both the influence of the ship within the field-of-view and the sun glitter. Mobley (1999) suggested a nadir angle of 40° and an azimuth angle of 135° away from the sun as the optimal direction. Unfortunately, sensors mounted in fixed positions onboard a moving ship experience very varying viewing directions with regard to the sun, and it may still be useful to have simple methods for estimating the different types of reflected radiance. In an on-going co-project with the Norwegian Institute for Water Research other angles than the nadir direction are studied. It is considered if observations in the ultraviolet and near infrared, where the water-leaving radiance in coastal water usually will be very small compared to the surface-reflected radiance, can be utilized for correction purposes. It has been demonstrated in this paper that if the ratios $L_{r,sky}/L(0^{\circ})$ and $L_{r,sun}/E_{sun}$ are known at one wavelength, their values at other wavelengths can be estimated. Since this is valid for the zenith-directed reflectance, it may possibly be applied to other directions as well.

References

Aas, E.: Calibration of a marine radiance and colour index meter, Rep. No. 87, Dept. Geophys., Univ. Oslo, 1993.

Aas, E. and Høkedal, J.: Reflection of spectral sky irradiance on the surface of the sea and related properties, Remote Sens. Environ., 70, 181–190, 1999.

Aas, E. and Højerslev, N. K.: Analysis of underwater radiance observations: Apparent optical properties and analytic functions describing the angular radiance distribution, J. Geophys. Res., 104, 8015–8024, 1999.

Aas, E., Højerslev, N. K., and Høkedal, J.: Conversion of sub-surface reflectances to above-surface MERIS reflectance, Int. J. Remote Sens., 30, 5767–5791, 2009.

Aas, E., Højerslev, N. K., and Lundgren, B.: Spectral irradiance, radiance and polarization data from the Nordic Cruise in the Mediterranean Sea during Jun–Jul 1971, Rep. No. 102, Dept. Geophys., Univ. Oslo, Norway, 1997.

Aas, E. and Korsbø, B.: Self-shading effect by radiance meters on upward radiance observed in coastal waters, Limnol. Oceanogr., 42, 968–974, 1997.

OSD
7, 1059–1102, 2010

Abramowitz, M. and Stegun, I. A.: Handbook of Mathematical Functions, Dover Publ., New York, 1970.
Adams, J. T., Aas, E., Højerslev, N. K., and Lundgren, B.: Comparison of radiance and polarization values observed in the Mediterranean Sea and simulated in a Monte Carlo model, Appl. Optics, 41, 2724–2733, 2002.
Cox, C. and Munk, W.: Statistics of the sea surface derived from sun glitter, J. Mar. Res., 13, 198–227, 1954a.
Cox, C. and Munk, W.: The measurements of the roughness of the sea surface from photographs of the sun's glitter, J. Opt. Soc. Am., 44, 838–850, 1954b.
Frouin, R., Schwindling, M., and Deschamps, P.-Y.: Spectral reflectance of sea foam in the visible and near-infrared: in situ measurements and remote sensing implications, J. Geophys. Res., 101, 14361–14371, 1996.
Gordon, H. R. and Ding, K.: Self-shading of in-water optical instruments, Limnol. Oceanogr., 37, 491–500, 1992.
Gordon, H. R. and Wang, M.: Surface-roughness considerations for atmospheric correction of ocean color sensors – I: The Rayleigh-scattering component, Appl. Optics, 31, 4247–4260, 1992a.
Gordon, H. R. and Wang, M.: Surface-roughness considerations for atmospheric correction of ocean color sensors – II: Error in the retrieved water-leaving radiance, Appl. Optics, 31, 4261–4267, 1992b.
Højerslev, N. K. and Aas, E.: Spectral irradiance, radiance and polarization in blue Western Mediterranean waters, in Ocean Optics XIII, Proc., 22–25 Oct 1996, Halifax, Canada, SPIE Vol. 2963, 138–147, 1997.
Høkedal, J. and Aas, E.: Observations of spectral sky radiance and solar irradiance, Rep. No. 103, Dept. Geophys., Univ. Oslo, Norway, 1998.
Kattawar, G. W. and Adams, C. N.: Errors in radiance calculations induced by using scalar rather than Stokes vector theory in a realistic atmosphere-ocean system, in Ocean Optics X, Proc., 16–18 Apr 1990, Orlando, Florida, SPIE Vol. 1302, 2–12, 1990.
Koepke, P.: Effective reflectance of oceanic whitecaps, Appl. Optics, 23, 1816–1824, 1984.
Kokhanovsky, A. A.: Spectral reflectance of whitecaps, J. Geophys. Res., 109, C05021, doi:10.1029/2003JC002177, 2004.
Lauscher, F.: Sonnen- und Himmelstrahlung im Meer und in Gewässern, in: Handbuch der Geophysik, 8, Physik der Atmosphäre, edited by: Linke, F. and Möller, F., Gebrüder Born-

OSD
7, 1059–1102, 2010

traeger, Berlin, 723–768, 1955.
Lundgren, B.: On the polarization of the daylight in the sea, Rep. No. 17, Dept. Phys. Oceanogr., Univ. Copenhagen, 1971.
Mobley, C. D.: Estimation of the remote-sensing reflectance from above-surface measurements, Appl. Optics, 38, 7442–7455, 1999.
Monohan, E. C.: Oceanic whitecaps, J. Phys. Oceanogr., 1, 139–144, 1971.
Monohan, E. C. and O'Muircheartaigh, I. G.: Optimal power-law description of oceanic whitecap coverage dependence on wind speed, J. Phys. Oceanogr., 10, 2094–2099, 1980.
Monohan, E. C. and O'Muircheartaigh, I. G.: Improved statement of the relationship between surface wind speed and oceanic whitecap coverage as required for the interpretation of satellite data, in: Oceanography from Space, edited by: Gower, J. F. R., Plenum, New York, 751–755, 1981.
Monohan, E. C. and O'Muircheartaigh, I. G.: Whitecaps and the passive remote sensing of the ocean surface, Int. J. Remote Sens., 7, 627–642, 1986.
Moore, K. D., Voss, K. J., and Gordon, H. R.: Spectral reflectance of whitecaps: instrumentation, calibration, and performance in coastal waters, J. Atmos. Ocean. Tech., 15, 496–509, 1998.
Moore, K. D., Voss, K. J., and Gordon, H. R.: Spectral reflectance of whitecaps: their contribution to water-leaving radiance, J. Geophys. Res., 105, 6493–6499, 2000.
Mueller, J. L., Davis, C., Arnone, R., Frouin, R., Carder, K., Lee, Z. P., Steward, R. G., Hooker, S., Mobley, C. D., and McLean, S.: Above-water radiance and remote sensing reflectance measurement and analysis protocols, in: Ocean Optics Protocols for Satellite Ocean Color Sensor Validation, Revision 4, Volume III: Radiometric Measurements and Data Analysis Protocols, NASA/TM-2003–21621/Rev-Vol. III, 21-31, 2003.
Munk, W.: An inconvenient sea truth: spread, steepness, and skewness of surface slopes, Annu. Rev. Mar. Sci., 1, 377–415, 2009.
Nicolas, J.-M., Deschamps, P. Y., and Frouin, R.: Spectral reflectance of oceanic whitecaps in the visible and near infrared: aircraft measurements over open ocean, Geophys. Res. Lett., 28, 4445–4448, 2001.
Preisendorfer, R. W. and Mobley, C. D.: Albedos and glitter patterns of a wind-roughened sea surface, J. Phys. Oceanogr., 16, 1293–1316, 1986.
Tyler, J. E.: Radiance distribution as a function of depth in an underwater environment, Bull. Scripps Inst. Oceanogr., 7, 363–412, 1960.

OSD
7, 1059–1102, 2010

Walker, R. E.: Marine Light Field Statistics, Wiley, New York, 1994.
Whitlock, C. H., Bartlett, D. S., and Gurganus, E. A.: Sea foam reflectance and influence on optimal wavelength for remote sensing of ocean aerosols, Geophys. Res. Lett., 9, 719–722, 1982.
Wu, J.: Oceanic whitecaps and sea state, J. Phys. Oceanogr., 9, 1064–1068, 1979.
Zibordi, G. and Ferrari, G. M.: Instrument self-shading in underwater optical measurements: experimental data, Appl. Optics, 34, 2750–2754, 1995.

OSD
7, 1059–1102, 2010

Table 1. Statistical properties of radiance ratios. Deviations are from the mean value.

	$L_r/L(0^\circ)$			$L_{r,sky}/L(0^\circ)$			$L_{r,sun}/L(0^\circ)$			$L_{r,foam}/L(0^\circ)$		
$W[m\,s^{-1}]$	0	5	10	0	5	10	0	5	10	0	5	10
Mean value	0.0215	0.0348	0.0784	0.0215	0.0237	0.0260	0	0.0110	0.0333	0	0.0002	0.0191
Minimum value	0.0201	0.0232	0.0298	0.0201	0.0198	0.0206	0	0	0.0002	0	0.0000	0.0040
Maximum value	0.0220	0.1901	0.3884	0.0220	0.0253	0.0292	0	0.1672	0.3145	0	0.0005	0.0531
Standard deviation	0.0003	0.0261	0.0575	0.0003	0.0010	0.0018	0	0.0264	0.0494	0	0.0001	0.0137
Max. deviation	0.0014	0.1553	0.3100	0.0014	0.0039	0.0055	0	0.1563	0.2813	0	0.0003	0.0339

OSD
7, 1059–1102, 2010

Table 2. Ranges of θ_s where sun glitter can be neglected.

W [m s^{-1}]	$L_{r,sun}/L(0°)<0.002$ θ_s	$L_{r,sun}/L(0°)<0.001$ θ_s
0	≥37°	≥37°
1	≥37°	≥37°
2	≥47°	≥50°
3	≥55°	≥57°
5	≥65°	≥68°
10	≥78°	

OSD
7, 1059–1102, 2010

Table 3. Statistical properties of radiance ratios at different wavelengths.

Wavelength [nm]	W [m s^{-1}]	$L_{r,sky}/L(0°)$ all θ_s			$L_{r,sun}/L(0°)$ θ_s=37–60°	$L_{r,sun}/L(0°)$ θ_s=37–70°	$L_{r,foam}/L(0°)$ all θ_s
		0	5	10	5	10	10
405	Mean value	0.0213	0.0228	0.0243	0.0102	0.0216	0.0079
	Standard deviation	0.0004	0.0011	0.0016	0.0119	0.0189	0.0024
	Max. deviation	0.0012	0.0030	0.0037	0.0215	0.0350	0.0039
450	Mean value	0.0215	0.0234	0.0254	0.0094	0.0215	0.0106
	Standard deviation	0.0001	0.0005	0.0011	0.0124	0.0203	0.0038
	Max. deviation	0.0002	0.0008	0.0021	0.0227	0.0459	0.0059
520	Mean value	0.0215	0.0239	0.0262	0.0185	0.0419	0.0162
	Standard deviation	0.0003	0.0006	0.0008	0.0293	0.0467	0.0071
	Max. deviation	0.0007	0.0014	0.0013	0.0572	0.1005	0.0101
550	Mean value	0.0216	0.0241	0.0270	0.0093	0.0306	0.0214
	Standard deviation	0.0002	0.0008	0.0016	0.0121	0.0200	0.0101
	Max. deviation	0.0005	0.0018	0.0038	0.0214	0.0305	0.0158
650	Mean value	0.0216	0.0242	0.0272	0.0381	0.0730	0.0368
	Standard deviation	0.0004	0.0012	0.0021	0.0592	0.0860	0.0138
	Max. deviation	0.0009	0.0028	0.0050	0.1292	0.2415	0.0264

OSD
7, 1059–1102, 2010

Table 4. Relative RMS error of estimates in % by two different normalizations.

Wavelength [nm]	$L_{r,sun}/L(0^{\circ})$		$L_{r,sun}/E_{sun}$	
	$W=5\,m\,s^{-1}$	$W=10\,m\,s^{-1}$	$W=5\,m\,s^{-1}$	$W=10\,m\,s^{-1}$
405	70	69	12	8
450	246	113	5	6
520	148	140	12	4
550	185	118	8	12
650	387	128	21	4

OSD
7, 1059–1102, 2010

Table 5. Polynomials for $L_{r,sky}/L(0^\circ)$, $L_{r,sun}/E_{sun}$, and $E_{sky}/L(0^\circ)$ on the form $A+B_1\theta_s+B_2\theta_s^2$, where θ_s is in units of degrees.

	$L_{r,sky}/L(0^\circ)$ (θ_s=37–76°)									$E_{sky}/L(0^\circ)$ (θ_s=37–76°)		
	W=0 m s^{-1}			W=5 m s^{-1}			W=10 m s^{-1}					
Wavelength [nm]	A [10^{-2}]	B_1 [10^{-6}]	B_2 [10^{-8}]	A [10^{-2}]	B_1 [10^{-5}]	B_2 [10^{-8}]	A [10^{-2}]	B_1 [10^{-4}]	B_2 [10^{-6}]	A [10^{-1}]	B_1 [10^{-1}]	B_2 [10^{-3}]
405	2.08	5.61	5.45	2.08	3.36	6.85	1.72	1.93	−1.05	−8.86	1.65	−1.03
450	2.13	−3.63	9.57	2.03	7.57	−36.3	1.43	3.19	−2.12	−42.0	2.86	−1.95
520	2.23	−17.9	6.41	2.55	−3.81	15.6	2.06	1.86	−1.47	−30.9	2.66	−1.80
550	1.86	91.4	−67.7	1.43	29.3	−212	3.71	−3.45	2.98	−74.9	3.88	−2.44
650	1.57	192	−150	0.879	50.0	−390	0.125	8.09	−6.01	−64.4	3.54	−2.04

	$L_{r,sun}/E_{sun}$								
	W=3 m s^{-1} (θ_s=37–50°)			W=5 m s^{-1} (θ_s=37–60°)			W=10 m s^{-1} (θ_s=37–70°)		
All wavelengths	A [10^{-2}]	B_1 [10^{-4}]	B_2 [10^{-5}]	A [10^{-2}]	B_1 [10^{-4}]	B_2 [10^{-6}]	A [10^{-2}]	B_1 [10^{-4}]	B_2 [10^{-6}]
	2.25	−9.53	1.02	2.03	−7.06	6.16	1.99	−5.52	3.92

OSD
7, 1059–1102, 2010

Table 6. Estimates of the ratio between water-leaving and reflected radiances. W=1.5–7.5 m s^{-1}, θ_s=37–52°.

Wavelength [nm]		L_r/E_{tot} [10^{-3}]	L_w/E_{tot} [10^{-3}]	L_w/L_r
405	Mean value	2.8	1.3	0.5
	Standard deviation	1.1	0.7	0.3
450	Mean value	2.7	2.0	0.8
	Standard deviation	1.0	1.1	0.3
520	Mean value	2.1	2.9	2.0
	Standard deviation	1.2	1.1	1.4
550	Mean value	2.4	2.9	1.4
	Standard deviation	0.9	1.1	0.7
650	Mean value	1.7	0.8	0.7
	Standard deviation	1.1	0.6	0.6

OSD
7, 1059–1102, 2010

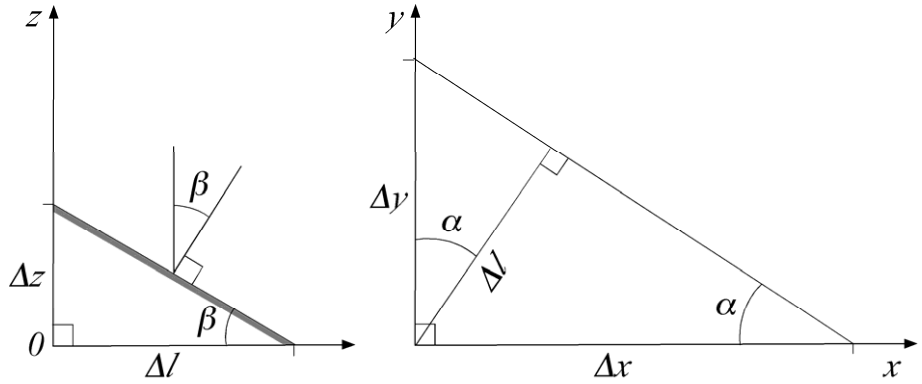

Fig. 1. Left: Vertical section in the steepest direction of the sloping surface. The grey line indicates the surface. Right: Projection of the sloping surface into the horizontal x-y-plane at z=0.

OSD
7, 1059–1102, 2010

Estimates of radiance reflected towards the zenith at the surface of the sea

E. Aas

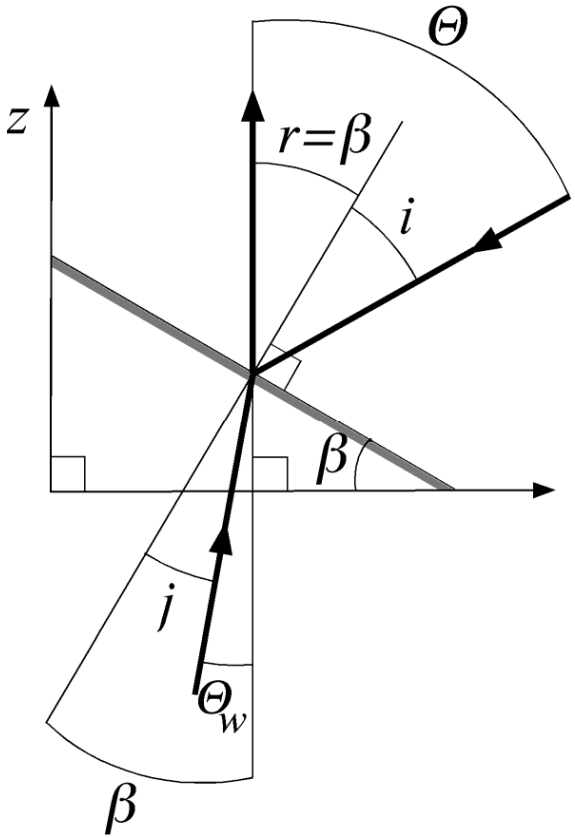

Fig. 2. Vertical section in the steepest direction of the sloping surface, indicated by the grey line. A ray from the zenith angle θ in the sky has an angle of incidence i and is reflected towards zenith in an angle of reflection r equal to i and slope angle β. A ray from the nadir angle θ_w in the sea has an angle of incidence j and is refracted through the surface at an angle of refraction r with a direction towards zenith.

OSD
7, 1059–1102, 2010

Estimates of radiance reflected towards the zenith at the surface of the sea

E. Aas

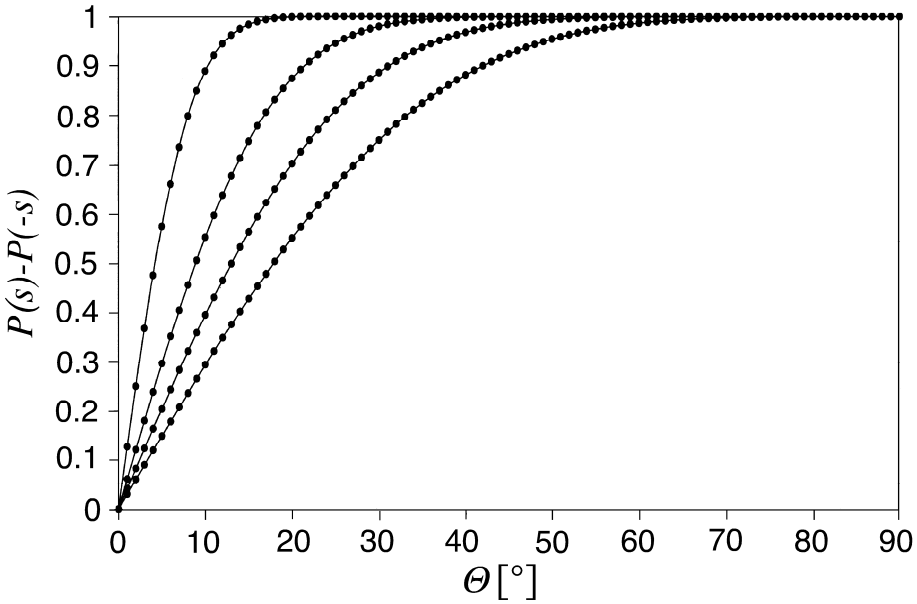

Fig. 3. The cumulative probability $P(s)-P(-s)$ as a function of the zenith angle θ in air corresponding to s. The curves represent from top to bottom the wind speeds 0, 2, 5 and 10 m s^{-1}.

OSD
7, 1059–1102, 2010

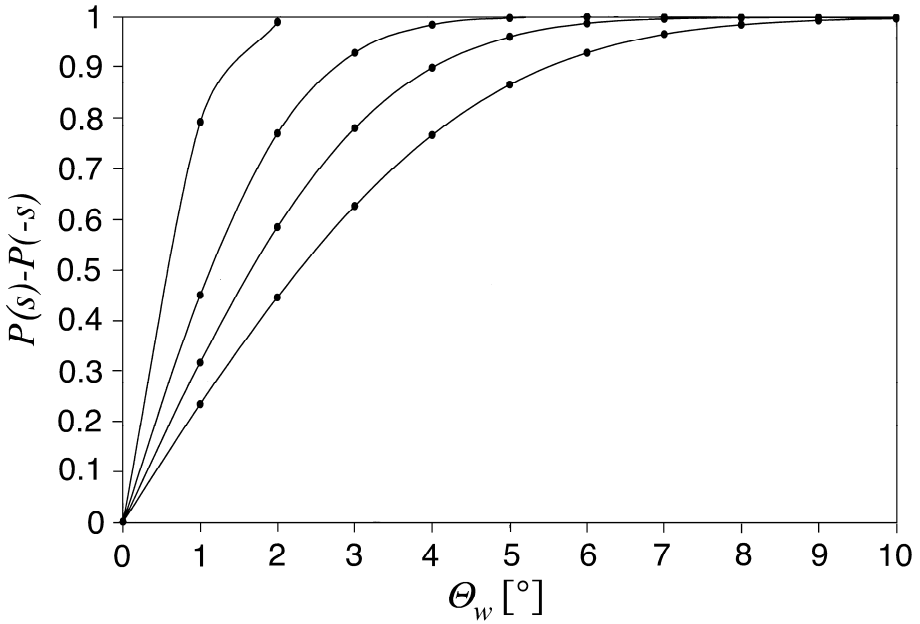

Fig. 4. The cumulative probability $P(s)-P(-s)$ as a function of the nadir angle θ_w in water corresponding to s. The curves represent from top to bottom the wind speeds 0, 2, 5 and 10 m s^{-1}.

OSD
7, 1059–1102, 2010

Estimates of radiance reflected towards the zenith at the surface of the sea

E. Aas

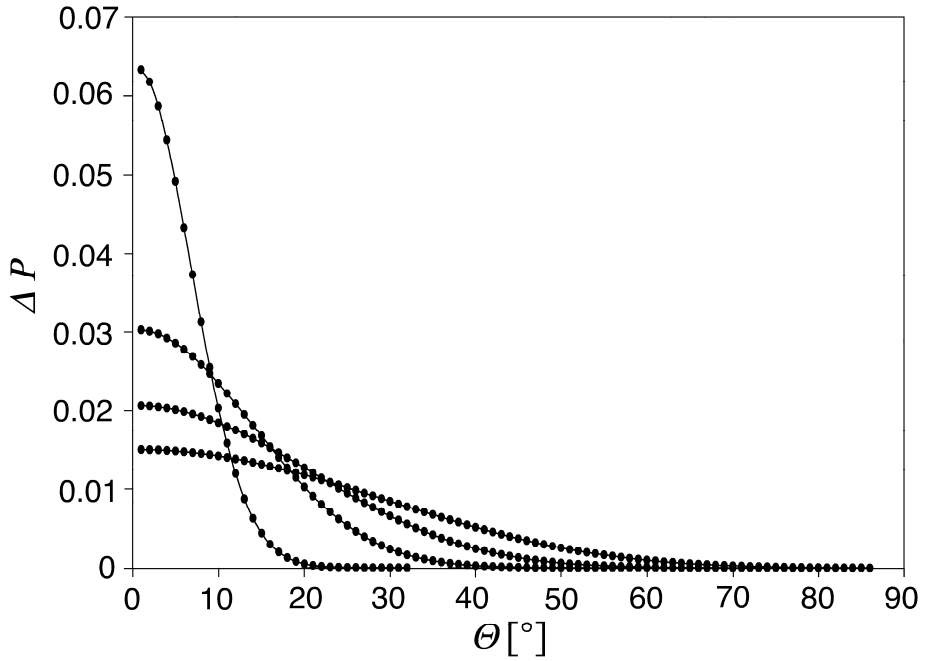

Fig. 5. The probability distribution ΔP as a function of the corresponding zenith angle θ in air. The curves represent from top to bottom in the left part of the graph the wind speeds 0, 2, 5 and 10 m s^{-1}.

OSD
7, 1059–1102, 2010

Estimates of radiance reflected towards the zenith at the surface of the sea

E. Aas

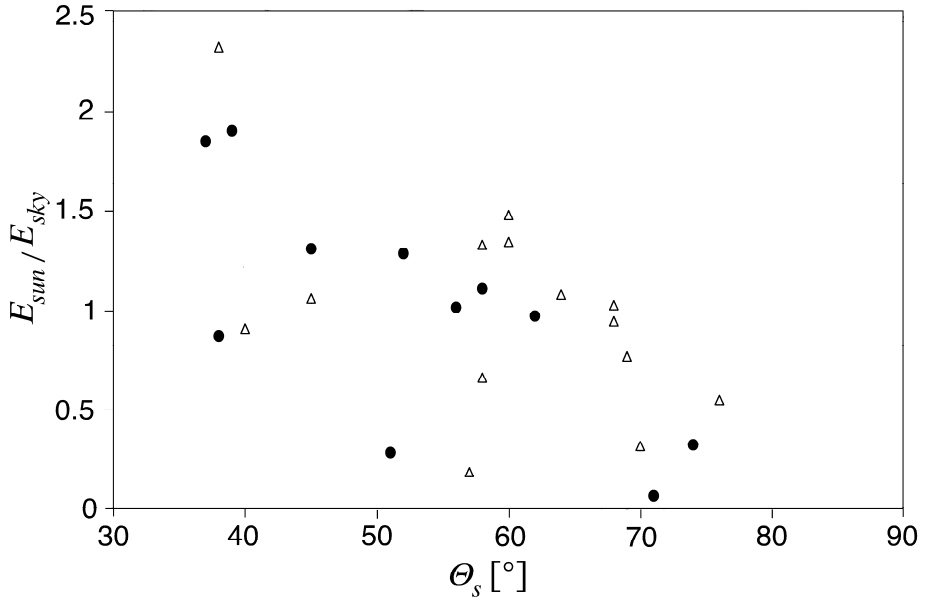

Fig. 6. The ratio E_{sun}/E_{sky} as a function of the solar zenith angle θ_s. The filled circles and open triangles represent 405 and 650 nm, respectively. The ratios are normalized against their mean values at these wavelengths.

OSD
7, 1059–1102, 2010

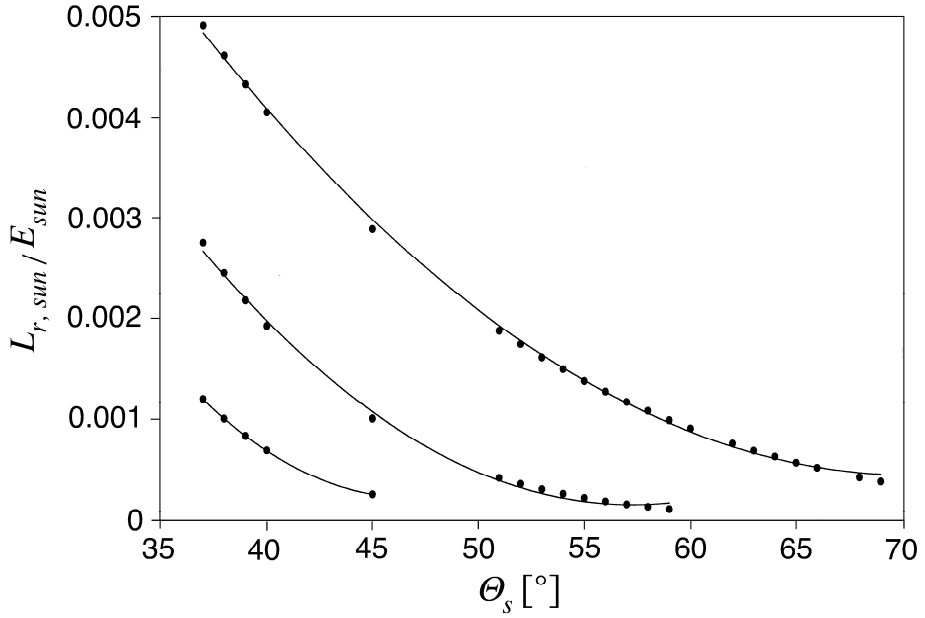

Fig. 7. The ratio $L_{r,sun}/E_{sun}$ as a function of θ_s, at the wavelengths 405, 450, 520, 550 and 650 nm. Only ratios greater than 0.0001 are taken into account. The best-fit lines represent, from bottom to top, the wind speeds 3, 5 and 10 m s^{-1}, and their polynomials are presented in Table 5.

OSD
7, 1059–1102, 2010

Estimates of radiance reflected towards the zenith at the surface of the sea

E. Aas

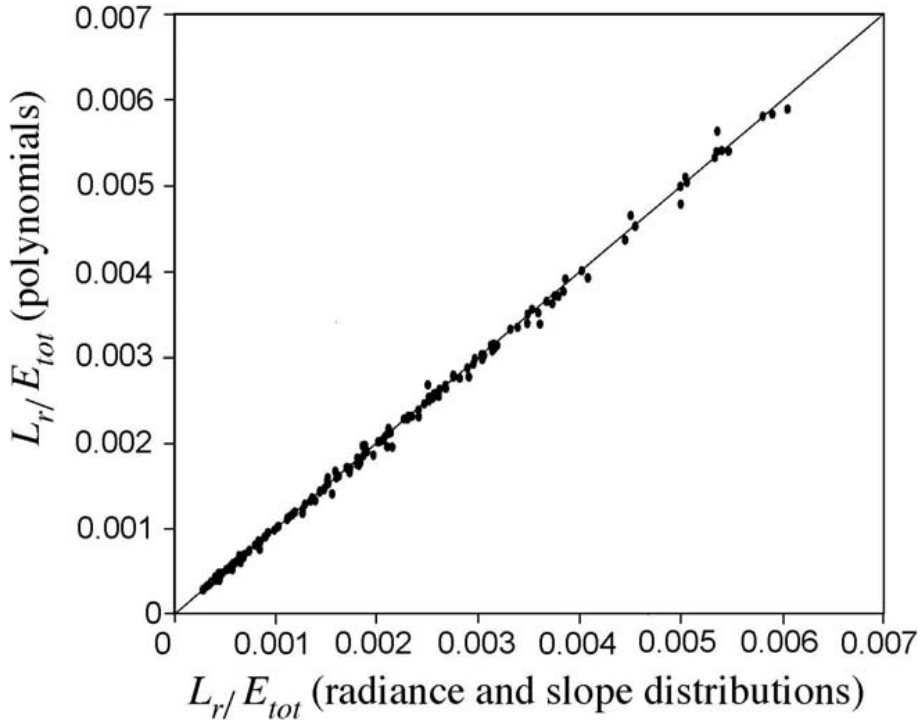

Fig. 8. The ratio L_r/E_{tot} obtained from the polynomials of Table 5 as a function of the same ratio calculated from the radiance and slope distributions, at the wavelengths 405, 450, 520, 550 and 650 nm, and at the wind speeds 0, 5 and 10 m s^{-1}.

OSD
7, 1059–1102, 2010

Estimates of radiance reflected towards the zenith at the surface of the sea

E. Aas